Angular and wavelength selectivity of parasitic holograms in cerium doped strontium barium niobate

Mostafa A. Ellabban
Institut für Experimentalphysik, Universität Wien, Boltzmanngasse 5, A-1090 Wien, Austria

Martin Fally[a)]
Institut für Experimentalphysik, Universität Wien, Boltzmanngasse 5, A-1090 Wien, Austria and Fachbereich Physik, Universität Osnabrück, D-49069 Osnabrück, Germany

Mirco Imlau
Fachbereich Physik, Universität Osnabrück, D-49069 Osnabrück, Germany

Theo Woike
Institut für Mineralogie und Geochemie, Universität zu Köln, D-50674 Köln, Germany

Romano A. Rupp
Institut für Experimentalphysik, Universität Wien, Boltzmanngasse 5, A-1090 Wien, Austria

Torsten Granzow
Fachbereich Material- und Geowissenschaften, Technische Universität Darmstadt, D-64287 Darmstadt, Germany

(Received 1 June 2004; accepted 21 September 2004)

The angular and wavelength selectivity of noise gratings in doped strontium barium niobate crystals for samples with two different thicknesses are investigated. We found that an offset in the optimum reconstruction angle with respect to the recording geometry occurs as a function of the thickness. This is a consequence of the unidirectional amplification. Thus the scattering intensity for the thinner sample is considerably lowered at the very recording conditions. We analyze the experimental results in terms of the kinematic theory of diffraction. © *2004 American Institute of Physics*. [DOI: 10.1063/1.1815383]

I. INTRODUCTION

The propagation of a laser beam through a photorefractive medium is always accompanied by photo-induced light scattering,[1] a nonlinear optical phenomenon. The origin of this process can be explained as follows: The incident light is scattered at optical inhomogeneities within the bulk crystal or irregularities at its surface. This scattered light interferes with the primary incoming beam and records a refractive-index pattern, i.e., parasitic volume holograms, via the photorefractive effect. As long as the waves diffracted from the recorded holograms are in phase with the primary scattered waves, they are amplified.[2] Usually it is assumed that this process proceeds until a steady state is established. The spatial dependence and the temporal evolution of the amplification process is governed by the photorefractive peculiarities of the material, e.g., the charge-transport mechanism, the sign of the charge carriers, etc. Despite the fact that this phenomenon has been known for a long time, holographic scattering in its entirety cannot be satisfactorily explained up to now. Therefore, experiments on substances of a different kind experiencing holographic scattering are continuously performed.[3–5] On one hand, some potential applications are based on holographic scattering, e.g., optical phase conjugation,[6] optical limiters,[7] novelty filters,[8] and incoherent-to-coherent conversion.[9] In addition, holographic scattering can be utilized to investigate material properties.[2,10–12] On the other hand, the presence of holographic scattering is considered to be a major obstacle for the applicability of photorefractive media as it corrupts the quality of any optical system. Therefore, eliminating or at least suppressing the effect of holographic scattering becomes a main goal in order to promote photorefractive crystals for industrial applications.[13,14]

In $LiNbO_3$:Fe, a representative for substances with a dominant local recording mechanism (photovoltaic effect), holographic scattering was characterized in detail by measuring the transmitted intensity as a function of the deviation from recording conditions.[15,16] In this contribution we extend these studies to $Sr_{0.61}Ba_{0.39}Nb_2O_6$:Ce (SBN61:Ce) crystals with a nonlocal photorefractive response (diffusion). In addition we pay particular attention to the angular dependence of the transmitted intensity for different sample thicknesses. The obtained experimental data are analyzed employing the kinematical theory of diffraction.

II. EXPERIMENTAL SETUP

We performed our studies on two single crystals of SBN61:Ce doped with 1.13 mol % cerium which were grown using the Czochralski method. The crystals are rectangular plates with their edges oriented along the crystallographic [100]- and [001] axes, the latter being parallel to the polar *c* axis. Table I presents the dimensions of the used SBN61:Ce crystals. The crystals were electrically poled by heating them to 140 °C, subsequently applying an electric

[a)]Electronic mail: martin.fally@univie.ac.at

TABLE I. Dimensions of the SBN61:Ce samples used, d denoting the thickness.

Sample	$a\|[100]\times d\|[010]\times c\|[001]$ (mm^3)
SBN1	$7.00\times1.91\times5.95$
SBN2	$7.29\times0.91\times6.31$

field of 350 V/mm along the c axis. Then the crystal was slowly (2 K/min) cooled down to room temperature and finally the electric field was removed. In order to record parasitic gratings, an extraordinarily polarized He–Ne laser beam at $\lambda_p=632.8$ nm ($I_p=0.39$ W/cm^2) was impinged perpendicularly onto the a-c face. Polarization state ($\vec{E}_p \| c$ axis) and intensity of the pump beam were adjusted by a combination of a $\lambda/2$ plate and a Glan–Thompson polarizer (see Fig. 1). A small fraction of the pump beam is directed onto a Si photodiode PD1 by the beam splitter BS3 to monitor the intensity of the pump beam. The transmitted intensity of the crystal is detected by photodiode PD2.

To reconstruct the parasitic holograms, the power of the laser beam is significantly reduced ($I_r \approx 0.4$ μW/cm^2) in order not to destroy the recorded holograms. The polarization state of the readout beam is kept the same as in recording, i.e., $\vec{E}_r \| \vec{E}_p \| c$ axis. To investigate the influence of the wavelength on the transmitted intensity, a frequency-doubled Nd:YAG laser ($\lambda_r=532$ nm), a diode laser ($\lambda_r=680$ nm), or the He–Ne laser is used for reconstructing the holograms. The readout beams were collinearly adjusted to the recording beam, as sketched in Fig. 1. The sample was fixed on an accurately controlled rotation stage ($\pm0.001°$) that permits rotations around two mutually perpendicular axes. The crystal can be rotated either around the c axis (ω rotation) or an axis perpendicular to the c axis (ϕ rotation).

III. EXPERIMENTAL RESULTS

A. Scattering pattern

Figure 2 displays the steady-state far-field scattering pattern of the sample SBN1 on a screen placed behind the sample in a plane perpendicular to the k_y direction. We relate the laboratory system and the crystallographic coordinate system by $[100]\|k_x$, $[010]\|k_y$, $[001]\|c\|k_z$. The scattered polarization-conserving intensity is completely depleted in the half space of the $+c$ axis, whereas it is distributed in the half space of the $-c$ axis. This is a characteristic feature of holographic scattering in a photorefractive material with a purely diffusion driven, i.e., nonlocal, charge-transport mechanism which yields the well-known unidirectional amplification.[17]

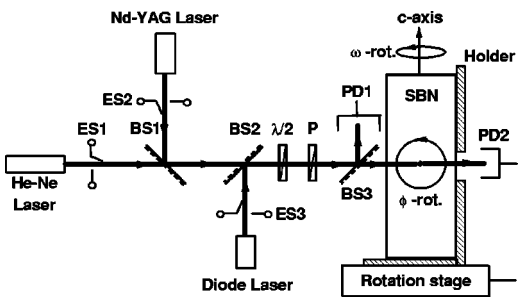

FIG. 1. Experimental setup for recording and reconstructing parasitic holograms. SF is a spatial filter, L is a lens, ES's are electromechanical shutters, BS's are beam splitters, $\lambda/2$ is a half-wave plate, P is a polarizer, SBN is the investigated crystal, and PD1 and PD2 are silicon photodiodes.

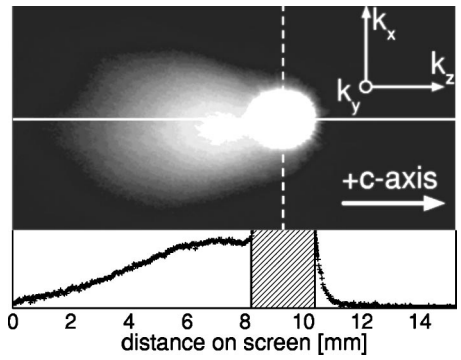

FIG. 2. Far-field intensity distribution of the amplified scattered light for a pump beam with $\lambda_p=632.8$ nm propagating through the sample SBN1 at room temperature. The $+c$ axis of the crystal points to the right. The pump beam is centered at the white spot shown to the right of the fanned light (hatched region). The screen was at a distance of 3 cm behind the sample. The scale at the bottom is in millimeters and is valid for the height and the width of the screen. The bottom graph depicts the intensity distribution along the white line indicated in the photograph. The dashed line represents the border between positive and negative c half space.

B. Reconstruction of parasitic holograms

As a first step after recording parasitic holograms, we performed measurements of the transmitted intensity $T(\phi;\lambda_r)$ as a function of the rotation angle ϕ, using different readout wavelengths as shown in Figs. 3(a) and 3(b). The

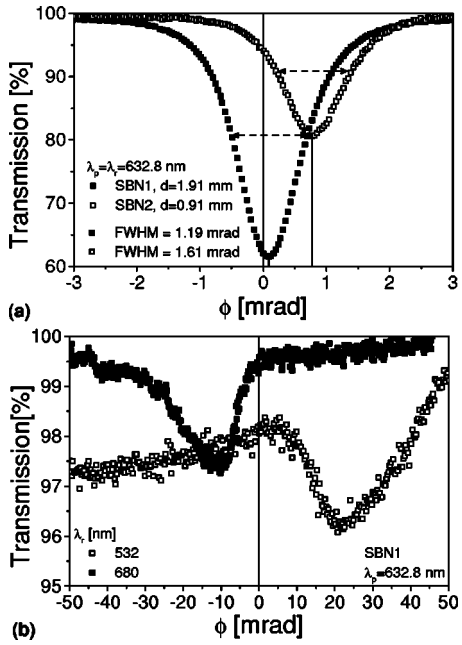

FIG. 3. Transmission as a function of the rotation angle ϕ at (a) $\lambda_r=\lambda_p=632.8$ nm for parasitic holograms written in SBN1 and SBN2 and at (b) $\lambda_r \neq \lambda_p$ during the reconstruction of parasitic holograms recorded in the sample SBN1. Note the difference in the scale of transmission in both figures. All rotation angles are given inside the crystal throughout this paper. $\phi=0$ denotes the recording geometry.

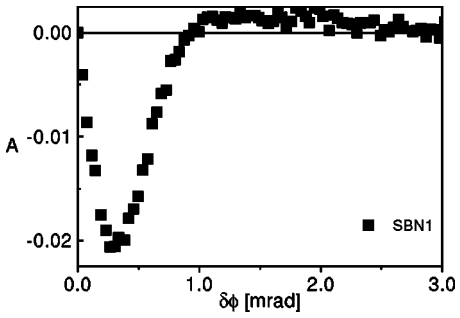

FIG. 4. Asymmetry parameter $A(\delta\phi)$ deduced from the experimental data for SBN1.

transmission is corrected for absorption and reflection, using the refractive and absorption indices known from literature.[18] For $\lambda_p=\lambda_r$, the minimum position of transmission astonishingly does not occur at the recording angle but is slightly shifted towards the positive sense of rotation. In other systems investigated so far, it is known that the minimum position of transmission ϕ_0 occurs at the recording angle provided that the recording and the readout conditions are identical.[15] Moreover, the transmission curve is not symmetric with respect to the minimum position ϕ_0. Here, we introduce an asymmetry parameter $A(\delta\phi)=[T(\delta\phi)-T(-\delta\phi)]/[T(\delta\phi)+T(-\delta\phi)]$ with $\delta\phi=\phi-\phi_0$. Figure 4 depicts $A(\delta\phi)$ obtained from the experimental results for the sample SBN1. For $\lambda_r>\lambda_p$ and $\lambda_r<\lambda_p$, a single minimum of transmission occurs at $\phi\neq 0$. Note that in the first case, $\phi_0<0$, whereas in the latter, $\phi_0>0$.

When studying the effect of the crystal thickness on holographic scattering, we obtained a quite surprising result. As expected, the full width at half maximum (FWHM) of the transmission curves depends on the crystal thickness when performing a ϕ rotation, as shown in Fig. 3(a): the FWHM is inversely proportional to the thickness.

The most distinct feature of that measurement, however, is a shift of the minimum's position from zero as a function of the crystal thickness, i.e., $\phi_0\neq 0$, even if the recording and reconstructing conditions are identical. The thinner the sample, the larger the magnitude of the shift. As can be seen from Fig. 3(a), the transmission changes from about 60% to 95% at $\phi=0$ for the crystals SBN1 and SBN2 with different thicknesses of 1.9 and 0.9 mm, respectively. For a qualitative understanding of the above-mentioned features, we decided to employ the concept of Ewald sphere[15,19,20] (cf. Sec. IV), rather than a more complex approach using coupled-wave analysis in Monte Carlo simulations which was presented only recently to describe similar experimental results.[21]

To complete the study, a measurement of the angular dependence of the transmitted intensity $T(\omega;\lambda_r)$ for a rotation around the c axis and different reconstruction wavelengths was performed (ω rotation) in the same way as for the ϕ rotation. Basically the transmission curves are symmetric with respect to the origin $\omega=0$ and the minimum transmission occurs at $\omega_0=0$ for $\lambda_r=\lambda_p$ [Fig. 5(a)]. However, in case of $\lambda_r\neq\lambda_p$, they exhibit two minima at $\omega=\pm\omega_0$ with the relative depth of the minima and their position being a function of λ_r/λ_p [Fig. 5(b)]. A thickness dependence of the minima's position cannot be observed [Fig. 5(a)].

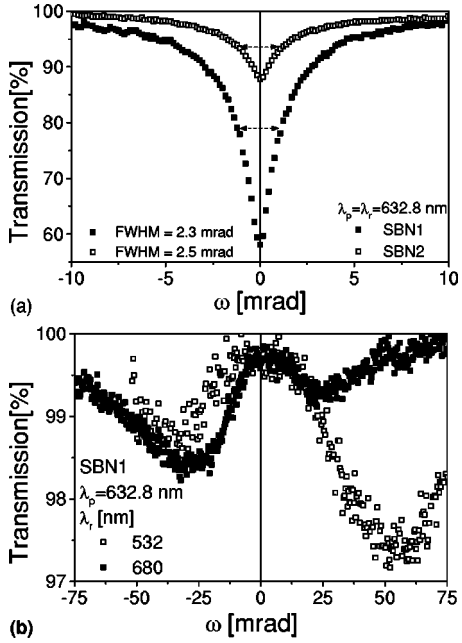

FIG. 5. Transmission as a function of the rotation angle ω at (a) $\lambda_r=\lambda_p=632.8$ nm for parasitic holograms written in SBN1 and SBN2 and at (b) $\lambda_r\neq\lambda_p$ during the reconstruction of parasitic holograms recorded in the sample SBN1.

IV. DISCUSSION

The Ewald-sphere construction concept of the kinematical theory of x-ray diffraction is well known in holography to describe and predict the angular geometry of holographic scattering[19,22] and the scattering circles in lithium niobate[20] as well as scattering rings and lines from volume gratings.[23] Recently, this model was employed to explain qualitatively the characteristic features of the angular, spectral, and polarization dependence of the transmitted intensity in the presence of parasitic holograms in $LiNbO_3$ or $Na_2[Fe(CN)_5NO]\cdot 2H_2O$, both media with a local photorefractive response.[4,15,16] As the Ewald-sphere model is a purely geometric construction without obvious correspondence to the actual behavior of the wave fields in the crystal in the presence of gratings during recording and reconstruction, it is expected to describe the essential features of any photorefractive medium irrespective of the type of recording mechanism.

The basic ideas of the model that are presented in detail in Ref. 15 are the following: In a first step, the pump beam (wave vector $\vec{k}_p$) is scattered from inhomogeneities. Those initially scattered waves (wave vector $\vec{k}_s$) interfere with the pump beam and lead to a complex scattered wave field represented by a complex interference pattern. Consequently refractive-index changes are induced in the photosensitive medium. These refractive-index changes are proportional to the product of modulation and linear-response function in the reciprocal space, if we assume small modulation, i.e., the amplitudes of the scattered wave fields are much less than the amplitude of the pump beam. The region of nonzero

refractive-index changes thus is confined to a narrow space around $\vec{k}_p - \vec{k}_s$ for isotropic media, i.e., to the surface of two spheres with the radius $|\vec{k}_p = 2\pi n/\lambda_p|$ centered at $\pm\vec{k}_p$.[15] These spheres are sometimes called the primary and conjugate images, as they are related to the recording of holograms and the generation of the optical phase conjugate, respectively. Therefore an efficient recording process can take place only for grating vectors for which energy and momentum are conserved. Hence a multitude of elementary gratings is recorded in the photorefractive material. At the beginning of the process, the amplitude of the refractive-index changes is quite small due to the low modulation. However, in a second step, successive diffraction from those elementary gratings leads to amplification and depletion of the scattered light into selective directions that depend on the specific response of the photorefractive medium under investigation. As a consequence the refractive-index change $\delta n(\vec{x})$ associated with a certain diffraction direction also increases or decreases. The Fourier transform of the refractive-index changes $\mathcal{F}\{\delta n\}(\vec{Q})$ is proportional to a function $S(\vec{Q})$, which we call a structure factor in analogy to crystallography. Its actual values are characteristic for the photorefractive material. For a standard diffraction problem, the scattered intensity then is $I_{sc}(\vec{Q}) = |S(\vec{Q})|^2$. However, for media with a nonlocal photorefractive response, holographic scattering is a self-diffraction process to be treated in the frame of dynamical holography. To understand the phenomenon, in addition to the intensities, the *phase relation* between the complex interference pattern and the generated refractive-index structure must be accounted for. This leads to a *unidirectional* energy transfer from the pump to the scattered beams and vice versa, with an amplitude variation proportional to $\exp(\pm\Gamma d)$. Scattered waves traveling towards the $\mp c$ direction are amplified or depleted, respectively, depending on the sign of charge carriers and the electro-optic coefficient.[24,25] Γ denotes the gain coefficient that specifies the coupling strength between the waves and is linearly proportional to $|S(\vec{Q})|$; d is the crystal thickness. By inspecting the scattering pattern in Fig. 2, we recognize that $I(\vec{Q})$ is extremely small for the half space $Q_z Q_x < 0$ compared to $Q_z Q_x > 0$, as expected from the aforementioned. Decreasing the thickness of the sample will also decrease the intensity ratio between those half spaces, thus resulting in a less asymmetric scattering pattern. We are aware of the fact that the gain coefficient depends on the scattering angle.[26,27] However, for the sake of simplicity, we assume that $I(\vec{Q}) = 0$ for $Q_z Q_x < 0$ and neglect this angular dependence, an approximation which is sufficient to understand the experimental results. Thus two hemispheres, the real and the conjugate images, result ("writing hemispheres"). As we do not discuss polarization effects in this contribution, the actually correct shape of hemiellipsoids[16] can be replaced simply by hemispheres.

At this point we have to discuss the conditions for an optimum reconstruction of our scattering pattern. As we are concerned with a multitude of gratings, with optimum conditions we mean that *all* of the gratings are reconstructed *at the same time*, i.e., they simultaneously fulfill Bragg's law.

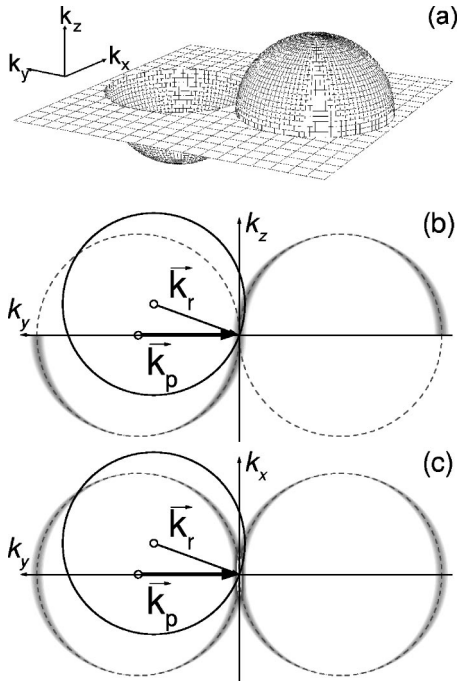

FIG. 6. Schematic view of the intensity distribution $I(\vec{Q}) \propto \exp(\pm\Gamma d)$ in the reciprocal space for SBN. (a) Three dimensional representation of the real (right hemisphere) and conjugate (left hemisphere) images, (b) cut perpendicular to the k_x and (c) k_z directions, respectively. Here, we assumed that the refractive-index changes are *equally* distributed along the hemispherical surface; the dashed lines represent exact Bragg matching, and the solid circle represents the corresponding cuts of the Ewald sphere for $\lambda_r > \lambda_p$.

This will then result in a maximum of diffracted intensity. Momentum and energy conservation in reciprocal space can be geometrically expressed as a sphere, the Ewald sphere, with radius $2\pi n/\lambda_r$ and its center at $\vec{k}_r$. As the crystal size is finite, efficient scattering occurs even in the case of slightly violating Bragg's law. Thus $I(\vec{Q})$ is smeared out in the reciprocal space by an extent ΔQ. The magnitude of the latter is given by Kogelnik's theory[28] and is inversely proportional to the thickness d of the sample. In Fig. 6 the blurred intensity distribution, which is strongly exaggerated for a better representation, and the Ewald sphere are shown for a typical experimental situation ($\lambda_p \neq \lambda_r, \vec{k}_p \neq \vec{k}_r$). The gray scale symbolizes the magnitude of $I(\vec{Q})$ and thus indicates those regions of the reciprocal space from which intensity can be supplied to a scattering process. For simplicity the angular dependence of the gain is neglected, so that the intensity distribution is constant along a sphere with radius $|\vec{k}_p|$. To reconstruct the parasitic holograms, an extraordinarily polarized readout wave is used that typically has different wavelengths λ_r or/and a different angle of incidence ϕ. Scattering of the readout beam takes place only if refractive-index changes occurred, i.e., $I(\vec{Q}) \neq 0$ *and* energy and momentum are conserved. The total scattered intensity therefore is proportional to the area of overlap between the Ewald sphere and the intensity distribution. Noticeable intensities show up only if the Bragg condition is simultaneously fulfilled for a significant number of parasitic holograms. In the experiment we intentionally violate the Bragg condition for some portion of the gratings and monitor the related intensity changes.

Analyzing the experimentally observed scattering pattern from Fig. 2 reveals that only grating vectors with a maximum spacing of about $2\pi/|\vec{K}_{max}|=3.5\ \mu$m do have a significant structure factor. These findings are implemented in the simulations for the total scattered intensity $I_S=1-I_T$, where we perform a surface integral of the intensity distribution over the Ewald sphere, $I_S=\oint I(\vec{Q})d\vec{A}$.

In reconstruction we are looking for the intersection of the Ewald sphere with the hemisphere of the primary image and its conjugate. This is expected to result in features which are specific for reconstructing parasitic holograms in SBN. These features can be summarized as follows:

(1) For reconstruction of parasitic holograms at $\lambda_p=\lambda_r$ and ϕ rotation, a single minimum occurs. The curve is slightly asymmetric with respect to the minimum position ϕ_0. Moreover, the latter depends on the thickness d of the sample. With increasing thickness the position approaches $\phi_0=0$ [see Fig. 3(a)].
(2) An asymmetric reconstruction curve with a single minimum $\phi_0\neq 0$ in the case $\lambda_r\neq\lambda_p$ is found. The position of the minimum depends on the ratio λ_r/λ_p and the thickness d. Note that the sign of ϕ_0 (for a sufficiently thick sample) depends on whether $\lambda_r>\lambda_p$ or $\lambda_r<\lambda_p$ [see Fig. 3(b)].
(3) For ω rotation and $\lambda_r=\lambda_p$, a symmetric reconstruction curve with one minimum at $\omega_0=0$ is revealed, regardless of the thickness.
(4) A double minimum structure for ω rotation is obtained in the case $\lambda_r\neq\lambda_p$ with the maximum of transmission at $\omega=0$. This resembles the results for ϕ rotation in $LiNbO_3$ (Ref. 15) (see Fig. 5).
(5) The FWHM is a function of the rotation axis (ϕ,ω) and thickness d.

Items 1–4 can be understood in the frame of the model.

Let us start the explanation with a magnification of the structure factor and the Ewald sphere in the vicinity of reciprocal space's origin in the k_y-k_z plane, i.e., Fig. 6(a). We recall that the scattered intensity I_S is given by integrating the structure factor over the surface of the Ewald sphere. The solid line in Fig. 7 indicates the latter at the very recording conditions, whereas the dashed and dotted lines represent the sphere for a deviation of $\phi=\pm\varphi$. From this figure it is clear that a slight rotation $-\varphi$ of the crystal in the negative sense, i.e., towards the $+c$ axis, results in an additional contribution of scattered intensity from the conjugate image. In contrast for a rotation $+\varphi$ the overlap area is smaller. This results in an asymmetry for the transmission curve relative to the minimum position (see Fig. 4).

In the preceding section we made use of the energy and momentum conservation laws to deduce the region in reciprocal space in which recording of gratings is principally allowed. Then we suggested to restrict this area to the half spaces $Q_xQ_z>0$ as SBN cannot exhibit holographic gain in both $+c$- and $-c$ direction (see Fig. 6). In addition we have to account for the fact that the gain strongly decreases with decreasing grating spacing,[27] i.e., larger diffraction angles. Therefore, the parasitic gratings are effectively recorded only

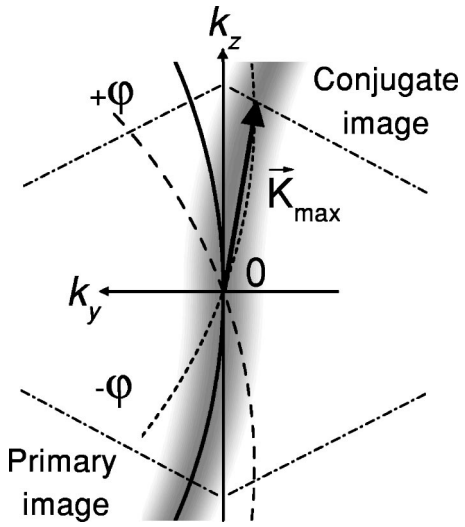

FIG. 7. Schematic view of the structure factor near the origin of reciprocal space for SBN in a cut perpendicular to k_x. The lines represent the Ewald spheres for $\lambda_r=\lambda_p$ at $\phi=0,\pm\varphi$.

for rather small diffraction angles, i.e., $|\vec{K}|<|\vec{K}_{max}|$. Consequently the structure factor is prominent only in the very vicinity of the reciprocal space's origin. The corresponding grating vectors in this region—indicated by the dashed-dotted lines in Fig. 7—considerably contribute to scattering. The consequence is that the minimum position ϕ_0 of the transmission deviates from $\phi=0$. Moreover, by decreasing the thickness of the sample, the width of the structure factor increases and the overlapping regions, too. Hence, a thinner sample yields a larger shift ϕ_0. The asymmetry of the rocking curve for $\lambda_r=\lambda_p$ and its thickness dependence are a fingerprint for systems with unidirectional amplification. We suggest investigating the angular dependence of $LiNbO_3$ that exhibits much less asymmetric amplification because the dominant transport mechanism is due to the (local) photovoltaic effect. It is even questionable if the standard model of two-wave weak signal amplification[24] can be used to fairly understand holographic scattering at all. Several systems were discovered that exhibit holographic scattering for which amplification on that basis is simply forbidden by symmetry because those media are centrosymmetric[29] or even isotropic.[19,30] We would like to emphasize that in thin crystals of SBN, i.e., crystals for which $\phi_0\neq 0$, holographic scattering is considerably enhanced in case of reconstruction conditions other than the recording conditions [cf. Fig. 3(a)]. Holographic recording by a two-wave mixing scheme is therefore considerably facilitated in such samples.

Simulations for the angular, wavelength, and thickness dependence (ϕ rotation) in such a medium are depicted in Fig. 8. A qualitative agreement with the experimental data (Fig. 3) is evident. We are aware of the fact that for a quantitative comparison the actual structure factor must be accounted for. In the simple simulation performed we assumed a uniform distribution along $\vec{Q}=\vec{K}+\vec{k}_p$ and a cutoff grating vector $\vec{K}_{max}$, i.e., $S(\vec{Q})\equiv 0$ for $|\vec{Q}|>|\vec{K}_{max}|$.

The experimental data for ω rotation prove that the features described above stem from the unidirectional amplification along the $-c$ direction. Note that the curves shown in

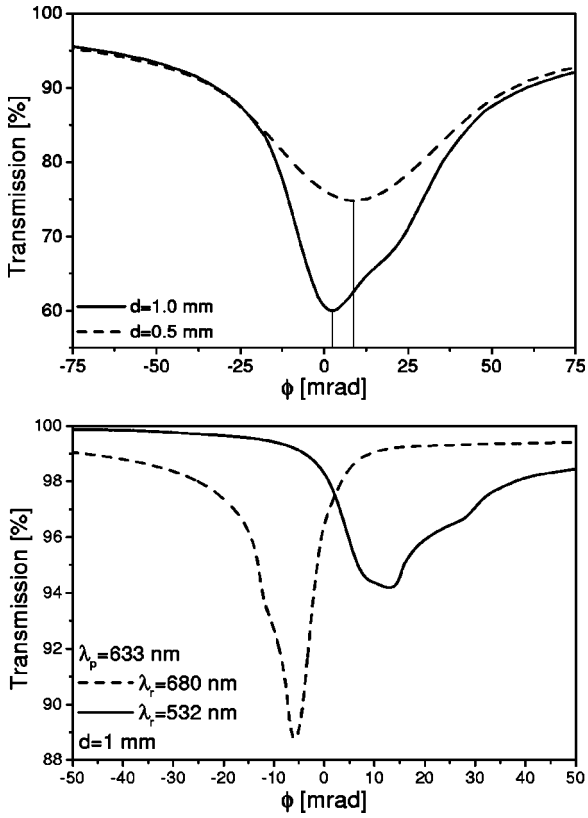

FIG. 8. Simulation of the transmission as a function of rotation angle ϕ for (a) $\lambda_r=\lambda_p$ and two different values of the sample thickness ($|\vec{K}_{max}|=0.2\ \mu m^{-1}$) and (b) $\lambda_r<\lambda_p$, $\lambda_r>\lambda_p$ with $|\vec{K}_{max}|=2\ \mu m^{-1}$.

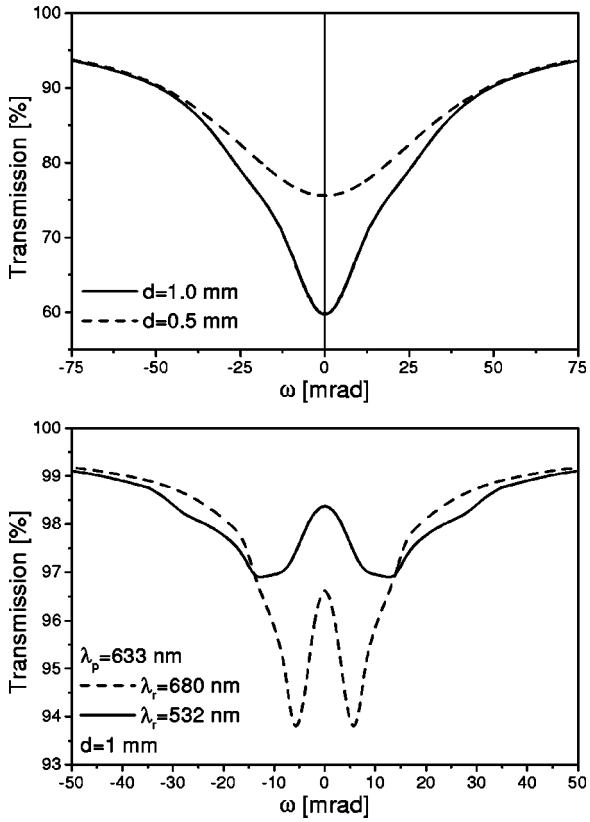

FIG. 9. Simulation of the transmission as a function of rotation angle ω for (a) $\lambda_r=\lambda_p$ and two different values of the sample thickness ($|\vec{K}_{max}|=0.2\ \mu m^{-1}$) and (b) $\lambda_r<\lambda_p$, $\lambda_r>\lambda_p$ with $|\vec{K}_{max}|=2\ \mu m^{-1}$.

Fig. 5(a) seem to be neither asymmetric nor do they exhibit a minimum value $\omega_0 \neq 0$. This is expected from the model, as the structure factor depicted in Fig. 6(b) is fully symmetric with respect to the k_y axis, a property which is probed by conducting this type of rotation. The corresponding simulation is shown in Fig. 9. The humps in the simulations can be explained by the fact that we use a sharp cutoff. This is a somewhat artificial way to account for the angular dependence of the gain and not the case in reality.

We found from the experimental data that the FWHM for ϕ rotation is less than for ω rotation. The simulation indicates that such a difference should not occur. We attribute this disagreement to the fact that $\vec{K}_{\max}$ is not the same in the planes k_x-k_y and k_y-k_z, respectively. This is an assumption which is confirmed by inspecting the scattering pattern from Fig. 2: The scattering is much more extended along the $-k_z$ direction than along the k_x direction. Moreover, as the curves are not fully symmetric (at least for the ϕ rotation), FWHM is not the proper measure for a comparison of the results.

The effect of the autogenerated parasitic holograms in SBN:Ce can be effectively minimized during reconstruction by using thin crystals or a different readout wavelength.

V. CONCLUSION

In summary, we have shown that the main features of the experimental results during reconstruction of parasitic holograms at different readout conditions in nonlocal recording media can be explained by using the kinematic theory of diffraction. It correctly predicts the occurrence of one or two minima under rotation around different crystallographic axes, the behavior when changing the wavelength, and the effect of sample thickness on the minimum position of transmission.

ACKNOWLEDGMENTS

Financial support by the Austrian Science Foundation FWF (P-15642) is acknowledged. One of the authors (M.F.) is grateful for a Mercator visiting professorship funded by the DFG (OS-55/12-1). This work was partially supported by the DFG (WO-618/3-4) and INTAS (01/0173). The authors thank Professor Dr. E. Tillmanns for continuous support.

[1] A. Ashkin, G. D. Boyd, J. M. Dziedzic, R. G. Smith, A. A. Ballman, A. A. Levinstein, and K. Nassau, Appl. Phys. Lett. **9**, 72 (1966).
[2] R. A. Rupp and F. W. Drees, Appl. Phys. B: Photophys. Laser Chem. **39**, 223 (1986).
[3] M. Goulkov, S. Odoulov, T. Woike, J. Imbrock, M. Imlau, E. Krätzig, C. Bäumer, and H. Hesse, Phys. Rev. B **65**, 195111 (2002).
[4] M. Imlau, T. Woike, D. Schaniel, J. Schefer, M. Fally, and R. A. Rupp, Opt. Lett. **27**, 2185 (2002).
[5] M. Y. Goulkov, T. Granzow, U. Dörfler, T. Woike, M. Imlau, and R. Pankrath, Appl. Phys. B: Lasers Opt. **76**, 407 (2003).
[6] J. Feinberg, Opt. Lett. **7**, 486 (1982).
[7] M. Cronin-Golomb and A. Yariv, J. Appl. Phys. **57**, 4906 (1985).
[8] M. Cronin-Golomb, A. M. Biernacki, C. Lin, and H. Kong, Opt. Lett. **12**, 1029 (1987).
[9] H.-Y. Lee, H.-F. Yau, and S.-W. Wang, Jpn. J. Appl. Phys., Part 2 **33**, L116 (1994).
[10] M. A. Ellabban, G. Mandula, M. Fally, R. A. Rupp, and L. Kovács, Appl. Phys. Lett. **78**, 844 (2001).

[11]M. Goulkov, M. Imlau, R. Pankrath, T. Granzow, U. Dörfler, and T. Woike, J. Opt. Soc. Am. B **20**, 307 (2003).
[12]M. Goulkov, T. Granzow, U. Dörfler, T. Woike, M. Imlau, R. Pankrath, and W. Kleemann, Opt. Commun. **218**, 173 (2003).
[13]H. Rajbenbach, A. Delboulbé, and J. P. Huignard, Opt. Lett. **14**, 1275 (1989).
[14]T. Volk, N. Rubinina, and M. Wöhlecke, J. Opt. Soc. Am. B **11**, 1681 (1994).
[15]M. Fally, M. A. Ellabban, R. A. Rupp, M. Fink, J. Wolfsberger, and E. Tillmanns, Phys. Rev. B **61**, 15778 (2000).
[16]M. A. Ellabban, R. A. Rupp, and M. Fally, Appl. Phys. B: Lasers Opt. **72**, 635 (2001).
[17]V. V. Voronov, I. R. Dorosh, Y. S. Kuz'minov, and N. V. Tkachenko, Sov. J. Quantum Electron. **10**, 1346 (1980).
[18]H. Landolt and R. Börnstein in *Ferroelectrics and Related Substances*, Group III-Condensed Matter, Vol. 36A, edited by Y. Shiozaki, E. Nakamura, and T. Mitsui (Springer-Verlag, Heidelberg, 2002), Chap. 6C–d2.
[19]M. R. B. Forshaw, Appl. Opt. **13**, 2 (1974).
[20]R. Magnusson and T. K. Gaylord, Appl. Opt. **13**, 1545 (1974).
[21]J. A. Frantz, R. K. Kostuk, and D. A. Waldman, J. Opt. Soc. Am. A **21**, 378 (2004).
[22]M. R. B. Forshaw, Opt. Commun. **8**, 201 (1973).
[23]S. I. Ragnarsson, Appl. Opt. **17**, 116 (1978).
[24]N. V. Kukhtarev, V. B. Markov, S. G. Odulov, M. S. Soskin, and V. L. Vinetskii, Ferroelectrics **22**, 961 (1979).
[25]M. P. Petrov, S. I. Stepanov, and A. V. Khomenko, *Fundamentals of Dynamic Holography*, Springer Series in Optical Sciences, Vol. 59 (Springer-Verlag, Berlin, 1991).
[26]A. P. Yakimovich, Opt. Spectrosc. **49**, 191 (1980).
[27]U. B. Dörfler *et al.*, Appl. Phys. B: Lasers Opt. **68**, 843 (1999).
[28]H. Kogelnik, Bell Syst. Tech. J. **48**, 2909 (1969).
[29]M. Imlau, T. Woike, R. Schieder, and R. A. Rupp, Phys. Rev. Lett. **82**, 2860 (1999).
[30]J. M. Moran and I. P. Kaminow, Appl. Opt. **12**, 1964 (1973).